Characterization of the 5.8 GHz V2I Radio Channel in an Underground Parking Garage

Pedro A. Vieira, Rodrigo A. Bilobran, Paulo V. G. Sampaio, Luiz A. R. Silva Mello, Rodrigo P. David, Leni J. Matos, Pedro V. G. Castellanos

***Abstract*— This study investigates radio signal propagation at 5.8 GHz in an underground parking garage for vehicle-to-infrastructure (V2I) communication, a widespread scenario present in urban centers. Broadband measurements were conducted using orthogonal frequency-division multiplexing (OFDM), enabling the characterization of the radio channel in terms of path loss (PL) and temporal dispersion. The power delay profile (PDP) was obtained via inverse Fourier transform of the channel impulse response (CIR). Multipath components were identified and compared using the constant false alarm rate (CFAR) and singular spectrum analysis (SSA) techniques. The results showed that the SSA technique is effective for multipath component identification.**

Keywords*— *CFAR, Delay spread, OFDM, radio propagation, SSA, V2I communication.

I. INTRODUCTION

Wireless vehicular communication is a promising solution for mitigating road safety risks and enhancing traffic management. Vehicular networks, which enable real-time information exchange between vehicles and infrastructure, can significantly reduce accidents, optimize traffic flow, and support the integration of autonomous vehicles [1].

In a dynamic environment, such as vehicular scenarios, constant vehicle mobility poses challenges for fast, safe, and effective communication. The movement of transmitters and receivers and the presence of obstacles cause radio signals to vary over time, which is influenced by multipath components from reflections on the ground, other obstacles, and vehicles. These multipaths increase angular scattering and propagation delay, resulting in significant signal fading [2]. Several authors have presented results on signal propagation loss in diverse vehicular environments such as highways, urban areas, and rural areas [1] [3]. Although these scenarios cover most of the vehicle communication situations, some environments require more detailed investigation, such as bridges, tunnels, and parking lots [4]. Enclosed environments such as parking garages are common in urban areas and must support vehicle-to-vehicle (V2V) and vehicle-to-infrastructure (V2I) communication. These structures, typically made of steel and concrete, with multiple floors and pillars, can be underground or elevated, thereby influencing the propagation conditions [5], [6]. Although many current mobile channel models are widely used in cellular systems, they often lack suitability for vehicular systems because of their distinct characteristics [7]. In [8] a survey on V2V communication models was conducted, and results in different scenarios were reported. In [9], the authors reviewed state-of-the-art channel measurements and modeling in the 60 GHz band. In [6], V2V communication in the 5 GHz band has concluded that the two-ray model closely matched the line-of-sight (LoS) conditions, while a PL exponent near 3 was observed in the non-line-of-sight (NLoS) conditions. In [10], measurements in an underground parking lot at 3.28 GHz and 5.03 GHz using ultra-wide band (UWB) yielded a PL exponent of 1.5. In [11] , an attenuation exponent of approximately 1.9 for NLoS in a 5.9 GHz garage environment, also reporting angular scattering results, with median values of approximately 45° for LOS and 60° for NLoS.

In this context, this study presents results obtained from measurements carried out at a frequency of 5.8 GHz in an underground parking environment characterized by concrete floors, ceilings, pillars and walls, developed within the scope of a doctoral research project [12]. The analysis focused on the characterization of the radio propagation channel through the PL and temporal dispersion parameters using OFDM transmitted signals.

The extraction of relevant multipath information from the measured PDP added to CFAR [13] and SSA [14] techniques, which were employed as filtering and denoising tools, provided results that were compared with those obtained by other authors.

This underground parking scenario was selected due to its high multipath potential, confined geometry, and widespread presence in urban centers, where reliable V2I communication is critical. These features provide a representative and challenging environment for evaluating signal dispersion. Underground garages combine metal and concrete structures with limited line-of-sight paths and high reflection density, posing unique challenges to signal analysis.

Section II describes the measurement environment and system configuration. Section III details the data analysis methodology, including SSA technique. Section IV presents the main results, and Section V provides conclusions and future research perspectives.

II. ENVIRONMENT AND MEASUREMENT CONFIGURATION

A. Measurement Setup

The system shown in Figure 1 was used to perform the measurements. On the transmission (Tx) side, an Anritsu MG3700A signal generator transmitted the OFDM signal connected to a Cisco AIR-ANT2547V-N omnidirectional antenna through a cable. The temporal dispersion of the channel was calculated from the PDP using an OFDM signal with the characteristics shown in Table I.

The data subcarriers of the OFDM signal were modulated by binary phase shift keying (BPSK), which has lower sensitivity to intersymbol interference (ISI) and intercarrier interference (ICI) [15], with bits of a pseudorandom sequence generated by a code that simulates a linear feedback shift register (LFSR).

Pedro A. Vieira, Rodrigo A. Bilobran, Paulo V. G. Sampaio, Leni J. Matos, Pedro V. G. Castellanos, Departamento de Engenharia de Telecomunicações da Universidade Federal Fluminense, Niterói, Brazil, e-mail: pavieira@id.uff.br, rbilobran@id.uff.br, paulo s@id.uff.br; lenijm@id.uff.br, pcastellanos@id.uff.br; Luiz A. R. Silva Mello, Centro de Estudos em Telecomunicações da Pontifícia Universidade Católica do Rio de Janeiro, RJ, Brazil, e-mail: larsmello@puc-rio.br; Rodrigo P. David, Inmetro, Rio de Janeiro, Brazil, e-mail: rpdavid@inmetro.gov.br

The ratio between the data subcarriers and total of subcarriers provides the bandwidth occupied by the data portion, and the variation of the spectrum amplitude will provide the spectral response of the channel. The inverse Fourier transform (IFFT) was then applied, resulting in an OFDM baseband (BB) signal, which was converted and loaded into the signal generator using Anritsu IQ Producer software.

TABLE I. *SETUP EQUIPMENT AND SPECIFICATIONS*

Parameter	Value
Number of subcarriers	4096
Data subcarriers	2920
Subcarrier spacing	13671.875 Hz
Sampling rate	56 Msps
OFDM Symbol Duration	82.28 us
Cyclic Prefix duration	9.14 us
Subcarrier modulation	BPSK
Bandwidth (data portion)	40 MHz
System resolution: spatial / temporal	5.36 m / 17.85 ns

To measure the signal, a Python program was developed to control the RSA306B spectrum analyzer using the Tektronix Application Programming Interface (API). The program configured the analyzer, defining the frequency, reception band, sampling rate, and sample duration, and saving the signal samples in-phase and quadrature (I/Q) variables. From this complex signal, the PDP is displayed in real time for local viewing and stored for subsequent temporal and other parameter analyses. At the reception (Rx) side, the setup included a Cisco AIR-ANT2547V-N antenna, which is the same as that used in the Tx, connected to an RG213 cable, and a Tektronix RSA306B spectrum analyzer for the received OFDM signal. Table II details the equipment gains and models, and Figure 1 illustrates the configuration of the measurement system.

TABLE II. *MAIN SETUP EQUIPMENT SPECIFICATIONS*

Item	Value
Transmit power	10 dBm
Tx cable loss (RG213), 1.5 m	2 dB
Rx cable loss (RG213), 1.5 m	2 dB
Antenna gain Tx/Rx (Cisco AIR-ANT2547V-N)	7.5 dBi

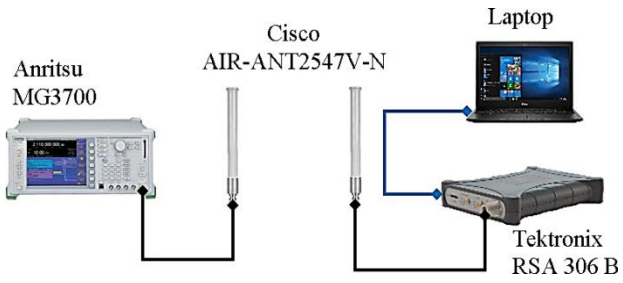

Fig. 1. System configuration for the measurement

B. Measurement Environment

The measurements were carried out in the underground parking garage of Shopping Nova América, located in the city of Rio de Janeiro, Brazil. This area consists of three lanes for vehicle circulation. Measurements were taken along the lane shown in Figure 2 and were used for access to parking spaces. Along each lane, there were five concrete pillars on each side, with dimensions of 50 cm by 100 cm. Each lane measured 7 meters in width and 42 meters in length. The site was completely enclosed, featuring a concrete wall at the end of the three lanes and another parallel to the lanes. At the end of the lane, there is also a concrete structure that houses the elevator shaft, which is marked in blue in Figure 2. The Tx was positioned in the lower-right corner of the environment, 8.5 meters from the beginning of the lane and 1.9 meters from the adjacent wall. Less than 25% of the parking spots were occupied by vehicles.

III. METHODOLOGY

Measurements were taken at eight fixed points located on the lane marked with a red "**x**" under the word "Point", followed by the number identifying each measurement location (from 1 to 8) as shown in Figure 2. The distance between measurement positions in the same lane was approximately 5 m. Figure 3 shows a photograph of measurement point 8, highlighting the receiving antenna, the laptop, some parked cars, the elevator structure on the right, and the transmitter (Tx) location. An initial measurement for calibration was made with the Receiving (Rx) antenna placed 5 m from Tx to verify that the propagation loss was close to the theoretical value given by the Friis equation [16], if there is an interference signal, and to measure the noise level, whose average value was –120 dBm. After verification, measurements were taken. In each position, the temporal, spectral, and multipath visualization of the signal was performed, followed by the capture and recording of the signal for a later analysis. The receiver configuration (RSA306B) was set to capture 20 OFDM symbols at each measurement point, which was sufficient to obtain the CIR in this controlled, low-traffic environment.

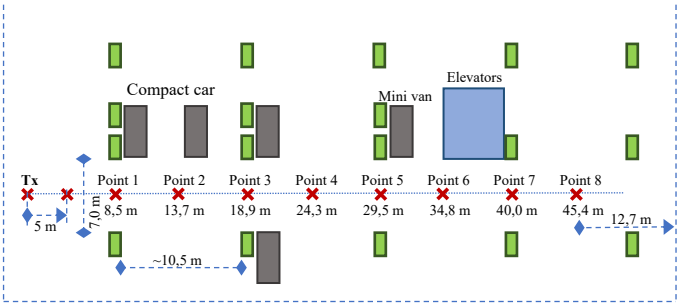

Fig. 2. Schema showing measured points in an underground parking lot at Shopping Nova América

Fig. 3. Photo of measurement point number 8 on lane of the underground parking garage

A. Signal spectrum

During the measurements, the variation in the signal level resulting from multipath was verified using a spectrum analyzer. Figure 4 shows the spectrum at each of the eight measured points whose selectivity, the product of the multipath effect, can be observed.

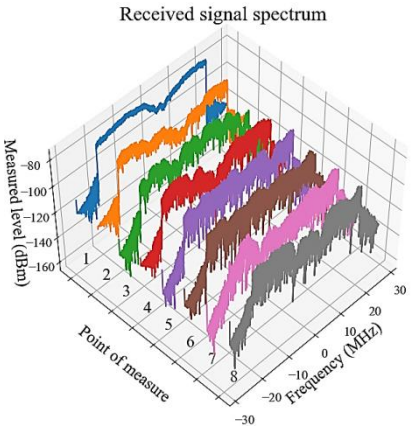

Fig. 4. Spectrum in each point of measurement

As shown in Figure 4, as Rx moves away from Tx (points 1–8), the spectrum variability increases owing to changes in the environmental composition at different locations. A decrease in the signal level and signal-to-noise ratio (SNR) can also be noted, and the values are listed in Table III.

TABLE III. *RECEIVED POWER, ATTENUATION AND SNR*

Point	Total band power level (dBm)	Att* from Tx to the point (dB)	Free space att* (dB)	Mean band power level (dBm)	SNR (band level)
1	-43.9	64.9	66.3	-79.6	40.4
2	-48.8	69.8	70.5	-85.6	34.4
3	-52.0	73.0	73.2	-89.3	30.7
4	-52.3	73.3	75.4	-90.2	29.8
5	-52.0	73.0	77.1	-89.2	30.8
6	-55.1	76.1	78.6	-92.3	27.7
7	-60.0	81.0	79.8	-99.0	21.0
8	-59.0	80.0	80.9	-97.8	22.2

**Attenuation*

B. Path loss

The PL was calculated at each measured point using wideband-measured signals. Figure 5 shows the curves comparing the calculated attenuation based on the measurements with those of free space.

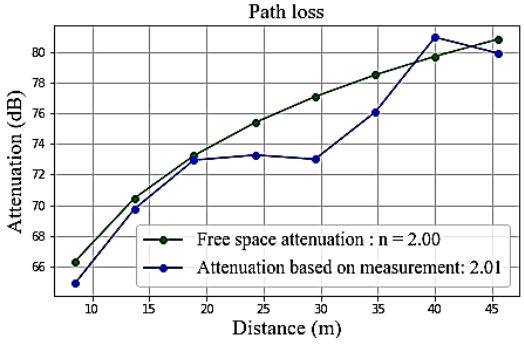

Fig. 5. Attenuation comparison

The results indicated that the attenuation factor was approximately 2, which is consistent with free-space propagation. The almost constant attenuation between 20 and 30 meters is due to the almost constant average signal level received in this section, which includes points 3, 4 and 5, with point 4 presenting the smallest number of obstacles on the sides.

C. Multipath

Using the collected OFDM signal, represented by in-phase and quadrature (IQ) samples, the OFDM spectrum was obtained via a Fourier transform. Based on this spectrum, the inverse Fourier transform was applied to obtain the CIR and the corresponding PDP. Figure 6 shows the average PDP of the 20 OFDM symbols at each of the 8 points.

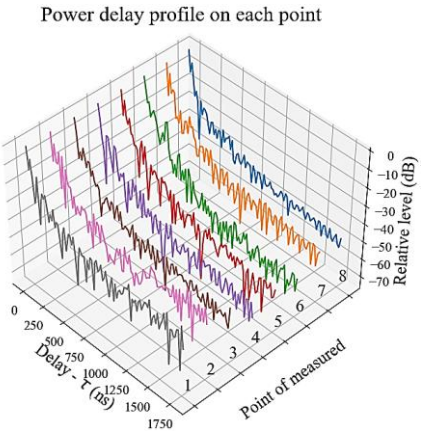

Fig. 6. PDP obtained in one of each point

The temporal dispersion parameters, calculated from the multipath identified from the PDP, average delay ($\bar{\tau}$), and RMS delay spread (τ_{rms}), are given by Eq. 1 and Eq. 2, where N is the total number of identified multipaths, τ_i is the delay of the $i-th$ path, and $P_h(\tau_i)$ is the relative power of the PDP for the delay τ_i in the $i-th$ path:

$$\bar{\tau} = \frac{\sum_{i=0}^{N-1} \tau_i P_h(\tau_i)}{\sum_{i=0}^{N-1} P_h(\tau_i)} \quad (1)$$

$$\tau_{rms} = \left[\frac{\sum_{i=0}^{N-1} P_h(\tau_i)(\tau_i - \bar{\tau})^2}{\sum_{i=0}^{N-1} P_h(\tau_i)}\right]^{\frac{1}{2}} \quad (2)$$

Figure 7 shows a processed PDP using the CFAR algorithm [13], which requires three PDP and a threshold to identify the valid multipaths.

Figure 8 shows the PDP processed by the SSA [14] technique that consists of four main steps: (i) embedding, in which the time series is transformed into a trajectory matrix using a sliding window and delay vectors; (ii) Singular Value Decomposition (SVD), which decomposes the trajectory matrix into orthogonal components (singular vectors and singular values); (iii) grouping, where components with similar characteristics are combined to separate the signal and the noise, usually based on the energy of the singular values; and (iv) reconstruction (Diagonal Averaging), which converts the grouped components back into a time series. From the reconstructed PDP, the multipath components can be identified as peaks located above a threshold, typically based on the highest energy singular values. From the multipath components

identified using CFAR and SSA techniques, the temporal spreading statistics, average delay and RMS delay spread [16], were calculated.

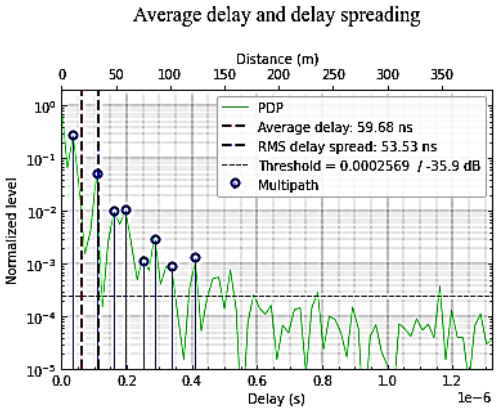

Fig. 7. PDP obtained by CFAR, average delay, RMS delay spread, and multipath at point 8

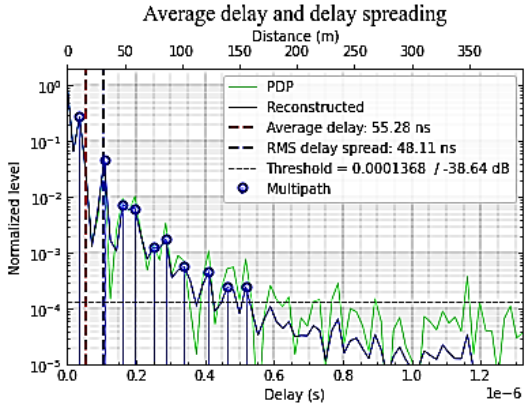

Fig. 8. PDP obtained by SSA, average delay, RMS delay spread, and multipath at point 8

IV. Results and Discussion

Although representative of real parking conditions, no vehicle movement was introduced during the measurement campaign. So, this study focused on static measurements with a fixed receiver position in a controlled environment. The effect of dynamic multipath variations due to moving objects or vehicles will be explored in future work through simulations and controlled dynamic trials.

Figure 9 shows the RMS delay spread obtained from the CFAR and SSA filtering techniques. From that figure, it is possible to observe that there is a greater difference between the techniques at point 1. Point 3 presents the maximum values for both techniques. Figure 10 shows the average delay in which the values and variation are very similar for both methods.

From Figure 9 and Figure 10, it is possible to observe the variation in the RMS delay spread and average delay values as the Rx moves away from the Tx. This behavior is due to the influence of the surrounding structures, which affect the signal levels of both the main and multipath components. For the RMS delay spread, the highest values occurred at point 3, decreased at point 4, and remained approximately the same at points 5, 6, 7, and 8. In terms of the average delay, there is a small increase from point 1 to 2; point 3 shows a significant increase, drops at point 4, and increases again at point 5, decreasing smoothly at points 6, 7, and 8. Analyzing the values of the RMS delay spread, it is possible to observe that the points with the largest values have cars parked nearby, points 3 and 5. Conversely, there is a drop in the value of point 4, where there are no vehicles nearby. Table IV shows the average number of multipath components in each point, RMS delay spread and average delay.

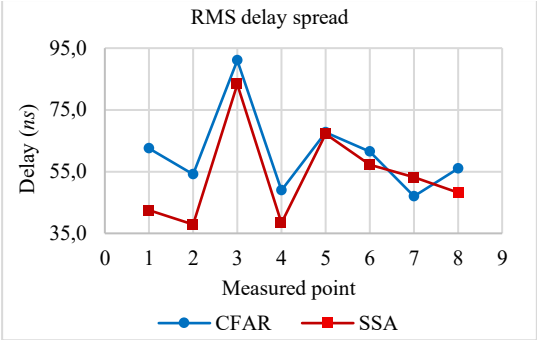

Fig. 9. RMS delay spread for CFAR and SSA filtering techniques

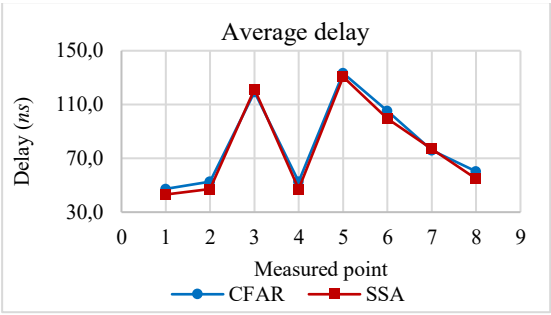

Fig. 10. Average delay for CFAR and SSA filtering techniques

TABLE IV. *Multipath, RMS Delay Spread and Average Delay*

	Multipath (mean value)		RMS Delay spread (ns)		Average delay (ns)	
Point	CFAR	SSA	CFAR	SSA	CFAR	SSA
1	22.0	17.6	62.5	42.5	47.3	43.1
2	11.1	12.6	54.1	37.9	52.7	47.3
3	7.1	68	91.0	83.3	119.2	121.4
4	8.9	9.0	48.9	38.4	52.6	47.3
5	5.6	6.9	67.7	67.2	133.3	130.5
6	8.1	9.3	61.4	57.3	105.4	99.6
7	7.7	13.1	47.0	53.1	76.0	76.9
8	8.9	10.0	55.9	48.2	60.2	54.8

In order to verify the values obtained by the calculation of the RMS delay spread, Table V presents a comparison with some environments studied: underground parking, and two other environments, Horizon parking garage [6], Auditorium [17], Covanca Tunnel [18], and Urban Environment [19]. Although they are distinct, they have characteristics and values of the RMS delay spread that can be used for comparative analysis. The RMS delay spread can vary significantly within the same type of environment due to factors such as layout, materials, and obstacle density. Generally, more reflections reaching the receiver (Rx) result in higher RMS delay spread. In tunnels, signals are partially guided by walls, ceiling, and floor produce

fewer reflections and shorter delay paths. Conversely, urban environments typically present larger, more spaced obstacles, increasing the number of reflections and the traveled path length, thus raising delay spread values. A comparison of tunnel and urban scenarios shows lower average delay and RMS delay spread in tunnels, confirming reduced multipath propagation.

TABLE V. *COMPARISON OF RMS DELAY SPREAD*

Environment	Observation	Frequency (GHz)	RMS Delay Spread (ns)
Underground parking garage	CFAR	5.8	61.1
	SSA		53.5
Horizon parking garage [6]	Empty garage	5.0	44.54
	Full garage		33.87
Auditorium [17]	Measured	1.95	58.02
	CFAR		54.16
	Simulated		52
Tunnel [18]		5.8	24.7
Urban [19]		0.7, 2.5, 3.5	61.0

The studied underground parking facility features numerous pillars, concrete surfaces, parked vehicles, and metallic infrastructure (e.g., ducts, conduits), creating a dense environment with extensive reflections.

V. CONCLUSION AND FUTURE DIRECTIONS

Broadband measurements were conducted using a transmitted OFDM signal, enabling the characterization of the radio channel in terms of path loss and temporal dispersion. This study investigated the propagation of radio signals in the 5.8 GHz band within an underground parking environment, aiming to analyze the behavior of the propagation channel for V2I communications by testing two techniques to identify valid multipath components.

Future studies will include controlled dynamic scenarios, either via measurement or simulation, to evaluate the performance of SSA and CFAR.

The PDP was obtained from the CIR, and the multipath components were estimated using the CFAR and SSA techniques. These techniques were applied to calculate temporal dispersion parameters and to perform a comparative analysis. The results showed that the average delay values were very similar for both techniques. The RMS delay spread exhibited distinct yet close values, with similar variation patterns and consistency with results reported by other authors. The findings indicate that SSA is a promising filtering technique for multipath identification. A literature review conducted in major scientific databases did not reveal prior applications of SSA for multipath component identification in the PDP obtained from radio channel sounding, suggesting the potential originality of this approach within the context of V2I communications. Future work will extend the measurement campaign to other conditions, including NLoS scenarios, multi-story garages, and outdoor areas. In addition, the impact of dynamic scenarios, such as moving vehicles, will be assessed.

ACKNOWLEDGEMENT

The authors would like to thank Shopping Nova América, located in Rio de Janeiro, and its administrative team for their support during the measurement campaign.

REFERENCES

[1] F. A. Rodriguez-Corbo, L. Azpilicueta, M. Celaya-Echarri, A. V. Alejos, e F. Falcone, “Propagation Models in Vehicular Communications”, IEEE Access, vol. 9, p. 15902–15913, 2021, doi: 10.1109/ACCESS.2021.3049884.

[2] D. Tse e P. Viswanath, Fundamentals of Wireless Communication, 1o ed. Cambridge University Press, 2005. doi: 10.1017/CBO9780511807213.

[3] Y. Fan et al., “Measurements and characterization for the vehicle-to-infrastructure channel in urban and highway scenarios at 5.92GHz”, China Commun., vol. 19, no 4, p. 28–43, abr. 2022, doi: 10.23919/JCC.2022.04.003.

[4] Cheng-xiang Wang, Xiang Cheng, e D. Laurenson, “Vehicle-to-vehicle channel modeling and measurements: recent advances and future challenges”, IEEE Commun. Mag., vol. 47, no 11, p. 96–103, nov. 2009, doi: 10.1109/MCOM.2009.5307472.

[5] R. Sun, D. W. Matolak, e P. Liu, “5-GHz V2V Channel Characteristics for Parking Garages”, IEEE Trans. Veh. Technol., p. 1–1, 2016, doi: 10.1109/TVT.2016.2601221.

[6] R. Sun, D. W. Matolak, e P. Liu, “Parking Garage Channel Characteristics at 5 GHz for V2V Applications”, em 2013 IEEE 78th Vehicular Technology Conference (VTC Fall), Las Vegas, NV, USA: IEEE, set. 2013, p. 1–5. doi: 10.1109/VTCFall.2013.6692343.

[7] W. Viriyasitavat, M. Boban, Hsin-Mu Tsai, e A. Vasilakos, “Vehicular Communications: Survey and Challenges of Channel and Propagation Models”, IEEE Veh. Technol. Mag., vol. 10, no 2, p. 55–66, jun. 2015, doi: 10.1109/MVT.2015.2410341.

[8] A. Molisch, F. Tufvesson, J. Karedal, e C. Mecklenbrauker, “A survey on vehicle-to-vehicle propagation channels”, IEEE Wireless Commun., vol. 16, no 6, p. 12–22, dez. 2009, doi: 10.1109/MWC.2009.5361174.

[9] R. He et al., “Propagation Channels of 5G Millimeter-Wave Vehicle-to-Vehicle Communications: Recent Advances and Future Challenges”, IEEE Veh. Technol. Mag., vol. 15, no 1, p. 16–26, mar. 2020, doi: 10.1109/MVT.2019.2928898.

[10] J.-Y. Lee, “UWB Channel Modeling in Roadway and Indoor Parking Environments”, IEEE Trans. Veh. Technol., vol. 59, no 7, p. 3171–3180, set. 2010, doi: 10.1109/TVT.2010.2044821.

[11] M. Yang et al., “V2V channel characterization and modeling for underground parking garages”, China Commun., vol. 16, no 9, p. 93–105, set. 2019, doi: 10.23919/JCC.2019.09.007.

[12] P. A. Vieira, “Validação de sistema de sondagem em faixa larga do canal rádio incluindo análise de técnicas de obtenção de perfil de potência de retardos e parâmetros de dispersão temporal”, Tese (doutorado), Universidade Federal Fluminense, Niterói, Brasil, 2025.

[13] E. S. Sousa, V. M. Jovanovic, e C. Daigneault, “Delay Spread Measurements for the Digital Cellular Channel in Toronto”, IEEE Transactions on Vehicular Technology, vol. 43, no 4, p. 837–847, 1994.

[14] N. Golyandina e A. Zhigljavsky, Singular Spectrum Analysis for Time Series. em SpringerBriefs in Statistics. Berlin, Heidelberg: Springer Berlin Heidelberg, 2020. doi: 10.1007/978-3-662-62436-4.

[15] S. Mohseni e M. A. Matin, “Study of the Sensitivity of the OFDM Wireless Systems to the Carrier Frequency Offset (CFO)”, IJDPS, vol. 4, no 1, p. 1–13, jan. 2013, doi: 10.5121/ijdps.2013.4101.

[16] T. Rappaport, Wireless Communications Principles and Practice, Second Edition. Prentice Hall, 2001.

[17] J. A. C. Braz et al., “Statistical characterization and simulation of a femtocell indoor radio channel”, em 2011 SBMO/IEEE MTT-S International Microwave and Optoelectronics Conference (IMOC 2011), Natal, Brazil: IEEE, out. 2011, p. 134–138. doi: 10.1109/IMOC.2011.6169409.

[18] A. Santos, L. Matos, P. Castellanos, e V. Mota, “Channel Characterization in V2I System inside a Tunnel in 5.8 GHz”, em 2021 SBMO/IEEE MTT-S International Microwave and Optoelectronics Conference (IMOC), Fortaleza, Brazil: IEEE, out. 2021, p. 1–3. doi: 10.1109/IMOC53012.2021.9624869.

[19] F. J. Oliveira e others, “Channel Characterization on Vehicle to Infrastructure Scenarios in 5.8 GHz”, em IEEE MTT-S Latin America Microwave Conference (LAMC), dez. 2018.